

Anomalous Hall effect and quantum criticality in geometrically frustrated heavy fermion metals

Wenxin Ding^{1,2,†}, Sarah Grefe^{3,2,†}, Silke Paschen⁴, and Qimiao Si²

¹*School of Physics and Optoelectronics Engineering,
Anhui University, Hefei, Anhui Province, 230601, China*

²*Department of Physics & Astronomy, Rice University, Houston, Texas 77005, USA*

³*Department of Physics & Astronomy, California State University, Long Beach, California 90840, USA*

⁴*Institute of Solid State Physics, Vienna University of Technology,
Wiedner Hauptstraße 8-10, 1040 Vienna, Austria*

Studies on the heavy-fermion pyrochlore iridate ($\text{Pr}_2\text{Ir}_2\text{O}_7$) point to the role of time-reversal-symmetry breaking in geometrically frustrated Kondo lattices. Here we address the effect of Kondo coupling and chiral spin liquids in a $J_1 - J_2$ model on a square lattice and a model on a kagomé lattice via a large- N method, based on a fermionic representation of the spin operators, and consider a new mechanism for anomalous Hall effect for the chiral phases. We calculate the anomalous Hall response for the chiral states of both the Kondo destroyed and Kondo screened phases. Across the quantum critical point, the anomalous Hall coefficient jumps when a sudden reconstruction of Fermi surfaces occurs. We discuss the implications of our results for the heavy-fermion pyrochlore iridate and propose an interface structure based on Kondo insulators to explore such effects further.

Heavy-fermion metals are prototypical systems to study quantum criticality [1–3]. The simplest model to describe these systems is a Kondo lattice, which comprises a lattice of local moments and a band of conduction electrons. The local moments are coupled to each other by the Ruderman-Kittel-Kasuya-Yosida (RKKY) interactions and are simultaneously connected to a band of conduction electrons through an antiferromagnetic (AF) Kondo exchange interaction (J_K). In recent years, it has been realized that the effect of geometrical frustration is a potentially fruitful but little-explored frontier. From a theoretical perspective, geometrical frustration enhances G , the degree of quantum fluctuations in the magnetism of the local-moment component, and a $J_K - G$ phase diagram at zero temperature has been advanced [4, 5]. Figure (1a) illustrates the proposed global phase diagram [4], which applies the notion of Kondo-destruction [6] to the parameter space that incorporates the frustration and related quantum fluctuation effects. From a materials perspective, there is a growing effort in studying frustrated Kondo-lattice compounds [7–14]

The pyrochlore heavy-fermion system $\text{Pr}_2\text{Ir}_2\text{O}_7$ is one such example. Both the measured magnetic susceptibility and specific heat [11] suggest the presence of Kondo coupling between the Ir d -electrons and the local f -moments of Pr. No magnetic order is found down to very low temperatures, suggesting that the f -moments of Pr develop a quantum spin liquid (QSL) ground state [11]. In addition, experiments found a sizeable zero-field anomalous Hall effect (AHE) for magnetic field applied along the [111] direction [15, 16], revealing a spontaneous time-reversal-symmetry-breaking (TRSB) state.

This system is of considerable theoretical interest [17–23]. With a few exceptions [24], the role of the Kondo effect has not been discussed in this context, and neither has its relationship with the observed quantum criticality.

Yet, the observation of a large entropy and a divergent Grüneisen ratio [25] clearly point to the importance of the Kondo coupling and the role of a proximate heavy-fermion quantum critical point (QCP). In the case of AF heavy-fermion systems, the normal Hall effect has been successfully used to probe the evolution of the Fermi surface across the QCP and, thereby, the nature of quantum criticality [3, 6, 14]. Given that the AHE is also intrinsically a Fermi surface property (other than contributions from fully occupied bands) [27], we are motivated to address whether it can serve as a diagnostic tool for the QCP in the present setting. In addition to elucidating the AHE, studying this issue promises to bring about the much-needed new understanding of quantum phases and their transitions in geometrically-frustrated heavy-fermion metals [14]. Given the complexity of the three-dimensional pyrochlore lattice, we will gain insights from related but simpler models.

In this Letter, we study both the frustrated $J_1 - J_2$ quantum Heisenberg model on a square lattice and the J_1 only model on the kagomé lattice with a Kondo coupling to conduction electrons. For the square lattice, we consider the regime of strong frustration where a chiral spin liquid (CSL) phase [28] becomes energetically competitive in a large- N limit (based on a Schwinger fermion representation of the spin operators; see below). The kagomé lattice, representing a layer perpendicular to the [111] direction of the pyrochlore lattice, is a two-dimensional network of corner-sharing triangles [Fig. (1d)] with a strong geometrical frustration. A CSL phase is found in a spin- $\frac{1}{2}$ model on the kagomé lattice [29]. Using the large- N limit [30], we will also study the CSL physics on this lattice. We develop the method to calculate the AHE in both a Kondo-destroyed (P_S) and a Kondo-screened (P_L) paramagnetic phase. We show that each phase may have a sizable AHE. Moreover, across a QCP, the AHE jumps

when the Fermi surface suddenly reconstructs.

Frustrated Kondo-lattice models We study the following Hamiltonian:

$$H = H_f + H_{d,0} + H_K \quad . \quad (1)$$

Here H_f describes a Heisenberg model. For the square lattice case, H_f includes both J_1 and J_2 couplings between the nearest neighbors ($nn, \langle \rangle$) and next-nearest neighbors ($nnn, \langle \langle \rangle \rangle$). We focus on the maximally frustrated case of $J_2/J_1 = 1/2$. For the kagomé case, the lattice is geometrically frustrated and it suffices for H_f to only contain the nn term. For both models with H_f alone, CSL states appear in the large- N limit [28, 31].

The local moments are coupled to a band of conduction electrons, described by $H_{d,0} = -\sum_{ij,\alpha} (t_{ij} d_{i\alpha}^\dagger d_{j\alpha} + h.c.)$, through an AF Kondo interaction J_K , specified by $H_K = J_K \sum_i \mathbf{s}_i \cdot \mathbf{S}_i$. Here, $\mathbf{s}_i = \sum_{\alpha,\beta} \frac{1}{2} d_{i\alpha}^\dagger \boldsymbol{\sigma}_{\alpha\beta} d_{i\beta}$ is the spin of the conduction electrons, with $\boldsymbol{\sigma}$ describing the Pauli matrices. We take $t_{\langle ij \rangle} = t = 1$ as the energy unit.

We use the Schwinger fermion representation for the f -moments $\mathbf{S}_i = \sum_{\alpha,\beta} \frac{1}{2} f_{i\alpha}^\dagger \boldsymbol{\sigma}_{\alpha\beta} f_{i\beta}$, with the constraint $\sum_{\alpha} f_{i\alpha}^\dagger f_{i\alpha} = 1$, so that $H_f = \sum_{\alpha,\beta,ij} \frac{J_{ij}}{2} f_{i\alpha}^\dagger f_{i\beta} f_{j\beta}^\dagger f_{j\alpha} - \frac{J_{ij}}{4} n_{i\alpha} n_{j\beta}$. In the large- N approach [31], the spin index $\alpha = 1, 2, \dots, N$, and the constraint is enforced by a Lagrangian multiplier λ_i . The Heisenberg and Kondo terms are decoupled by a Hubbard-Stratonovich (HS) transformation. The large- N limit leads to

$$H_{eff} = H_{QSL} + H_{d,0} + H_{K,eff} + E_c \quad , \quad (2)$$

with $H_{QSL} = -\sum_{ij,\alpha} \frac{J_{ij}}{2} (\chi_{ji} f_{i\alpha}^\dagger f_{j\alpha} + h.c.) - \sum_{i,\alpha} \lambda_i (f_{i\alpha}^\dagger f_{i\alpha} - 1/2)$, $H_{K,eff} = -\sum_{i,\alpha} \frac{J_K}{2} (\pi_i d_{i\alpha}^\dagger f_{i\alpha} + h.c.)$, and $E_c = \sum_{ij} N J_{ij} |\chi_{ij}|^2 / 2 + \sum_i N J_K |\pi_i|^2 / 4$. The HS fields are defined as $\chi_{ij} = \sum_{\alpha} \langle f_{i\alpha}^\dagger f_{j\alpha} \rangle$ and $\pi_i = \sum_{\alpha} \langle f_{i\alpha}^\dagger d_{i\alpha} \rangle$. Both can be decomposed into amplitudes and phases: $\chi_{ij} = \rho_{ij} e^{iA_{ij}}$, $\pi_i = \rho_{K,i} e^{iA_{K,i}}$. The Kondo parameter π_i can be taken to be real, with its phase absorbed into the field λ_i , i.e. $\pi_i \rightarrow \rho_{K,i}$.

By minimizing the total energy of H_{eff} in Eq. (2), we obtain the phase diagrams containing the chiral states, in which J_K tunes the system from the P_S to P_L phases (see Supplemental Material [32]). Across a second-order Kondo-destroyed $P_{S,chiral}$ to $P_{L,chiral}$ quantum phase transition, Fig. (1b), we consider a power-law form for the Kondo hybridization amplitude:

$$\rho_K(J_K) = \rho_r \left(\frac{J_K - J_{K,c}}{J_K} \right)^{1/2} \quad , \quad (3)$$

for $J_K > J_{K,c}$ and $\rho_K = 0$, for $J_K < J_{K,c}$. We take $J_{K,c}$ as the value where the $P_{L,chiral}$ state becomes energetically competitive and ρ_r to be the saturation value of ρ_K ; both values are adopted from the self-consistent calculation for a given set of (n_d, J_1) [32].

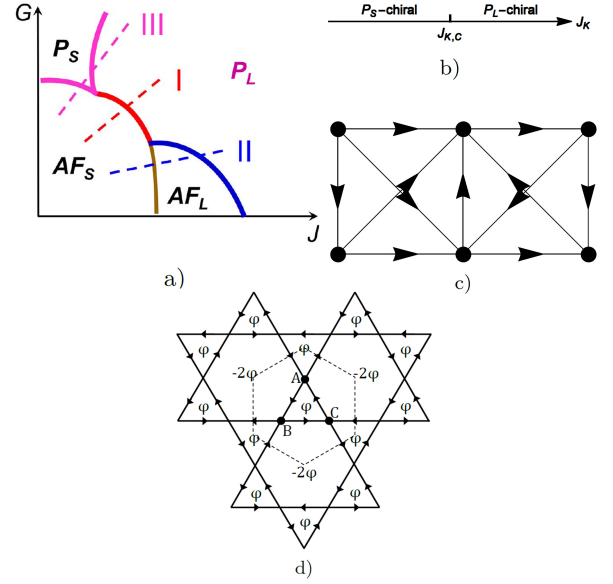


FIG. 1. (Color online) (a) The global phase diagram of Kondo lattice systems [4]; (b) In the highly frustrated regime (large, fixed G), J_K tunes through a Kondo-destruction QCP (at $J_{K,c}$) from a Kondo-destroyed chiral spin liquid ($P_{S,chiral}$) to a Kondo-screened phase ($P_{L,chiral}$). The χ fields of the square lattice are shown in the π -flux state (without the diagonal bonds) and the CSL state (c), and in the CSL state on the kagomé lattice (d): the arrows denote the sign of gauge field A_{ij} , and ϕ is the flux through a triangle.

Mechanism of the AHE - the Kondo destroyed P_S phase. In the Kondo-destroyed P_S phase, the static hybridization amplitude vanishes, $\langle \rho_{K,i} \rangle = 0$. However, we show that there are TRSB terms in the effective interactions among the conduction electrons, which are mediated by the spinons via Kondo couplings. Such terms yield a zero-field AHE.

We will single out the TRSB terms. The TRSB order parameter of the CSL is the spin chirality,

$$\hat{E}_{ijk} = \mathbf{S}_i \cdot (\mathbf{S}_j \times \mathbf{S}_k) \quad , \quad (4)$$

where the indices $\{i, j, k\}$ mark the three sites of an elementary triangle of the lattice. In the CSL state, $E_{ijk} = \langle \hat{E}_{ijk} \rangle = 2i(P_{ijk} - P_{ikj})$, where $P_{ijk} = \chi_{ij}\chi_{jk}\chi_{ki}$. On symmetry grounds, we expect E_{ijk} to be coupled to the composite chiral operator of the conduction electrons, $\mathbf{s}_i \cdot (\mathbf{s}_j \times \mathbf{s}_k)$. With this guidance, we obtain the coupling from integrating out the f -fermions and expanding in powers of J_K ; this can be represented by triangular diagrams (Supplemental Material [32]), similar to what is used in deriving a chiral current. We find

$$\begin{aligned} H_{chiral} &= \sum \frac{J_K^3}{3!} \underbrace{(\mathbf{s}_i \cdot \mathbf{S}_i)(\mathbf{s}_j \cdot \mathbf{S}_j)(\mathbf{s}_k \cdot \mathbf{S}_k)}_{\Delta\text{-loop contraction}} \\ &= \frac{J_K^3}{2 \times 3!} E_{ijk} \mathbf{s}_i \cdot (\mathbf{s}_j \times \mathbf{s}_k) \quad . \end{aligned} \quad (5)$$

In the kagomé case, the hexagons can also possess non-trivial fluxes. However, we can restrict the effective TRSB coupling for the conduction electrons to the lowest order in J_K , which corresponds to considering only the fluxes of the triangles.

The chiral interactions in H_{chiral} have a six-fermion form. We can decouple it by introducing a novel HS transformation that involves triangular diagrams described in the Supplemental Material[32]. We end up with an effective bilinear theory:

$$H_d = H_{d,0} + H_{d,1} \quad (6)$$

with

$$H_{d,1} = \sum_{ij} (g\phi_j^* \phi_i d_i^\dagger d_j + \phi_i^* G_{\phi,ij}^{-1} \phi_j + h.c.) \quad (7)$$

Hence, the ϕ -fields are constrained by the condition that, if they are integrated out, we obtain the same chiral interaction terms at $\mathcal{O}(g^3)$ by computing the same triangle diagrams. We then replace $\phi_j^* \phi_i$ by its expectation value $G_{\phi,ij}$ and arrive at

$$H_{d,1} \rightarrow \sum_{ij} (gG_{\phi,ij} d_i^\dagger d_j + h.c.) \quad (8)$$

It turns out that $G_{\phi,ij} = e^{-iA_{ij}}$, and g can be identified as $g = J_K(|E_{ijk}|/2)^{1/3}$. Because the bosonic Gaussian integral has a minus sign relative to its fermionic counterpart, $G_{\phi,ij}$ carries the opposite flux pattern to produce the same H_{chiral} when we integrate out the ϕ -fields. Physically, the flux (or chirality) pattern has the opposite sign to that of the CSL state, so that the antiferromagnetic Kondo coupling will lower the ground state energy. This effective Hamiltonian is adequate for qualitatively describing the AHE physics of our original Hamiltonian. Other non-chiral effective interactions would only renormalize the Fermi liquid parameters of the d -electrons for the P_S phase. We can then use the Streda formula [38, 39] to compute the AHE coefficient σ_{xy} : The involved quantities are the current operator of the conduction electrons $v_a(\mathbf{k}) = \partial_a H_d(\mathbf{k})$, the Berry curvature $\mathcal{F}_n^{xy}(\mathbf{k})$, and the Fermi function $f(\epsilon_n(\mathbf{k}))$ (Supplemental Material[32]).

Mechanism of the AHE - the Kondo screened P_L phase. In the P_L phase, the Kondo order parameter $\rho_{K,i}$ acquires a non-zero expectation value $\rho_K = \langle \rho_{K,i} \rangle$. There should still be an incoherent piece of the slave boson fields: $\rho_{K,i} = \rho_K + \pi'_i$. Moreover, we focus on the case where the chiral order survives in the P_L phase. By considering the same triangular diagrams now mediated by the incoherent part π'_i , the fluctuations of the Kondo order parameter still mediate chiral interactions similarly as in the P_S phase, but with a reduced weight. However, there is no spectral sum rule for the π'_i s to obtain this reduced weight readily. In the Supplemental Material [32], we use a slave rotor approach for the periodic Anderson

model to determine this factor. The effective Hamiltonian of the d -electrons becomes

$$H_d = H_{d,0} + [1 - (4J_K/U)\rho_K^2]H_{d,1} \quad , \quad (9)$$

where U is the onsite Hubbard repulsion. We fix $U = 2W$, *i.e.* twice the d -electron's bandwidth throughout the calculations. Keeping only the ρ_K part of H_K leads to the following effective Hamiltonian:

$$H_{P_L} = \Psi^\dagger \begin{pmatrix} H_{\text{CSL}} & -J_K \rho_K \mathcal{I} \\ -J_K \rho_K \mathcal{I} & H_d \end{pmatrix} \Psi \quad , \quad (10)$$

where \mathcal{I} is an identity matrix, and $\Psi^\dagger = (f^\dagger, d^\dagger)$. We have dropped the spin index, as there are no longer spin-flip terms. The Hamiltonian H_{P_L} is smoothly connected with H_d at the QCP. We then compute σ_{xy} from the Streda formula Eq. (S-22), noting that the current operators remains the same, *i.e.* $v_a(\mathbf{k}) = \partial_a H_d(\mathbf{k})$.

AHE and its evolution across the Kondo-destruction QCP. For the square lattice, we focus on the π -flux and the CSL states which are known to be closely competing in the pure $J_1 - J_2$ Heisenberg models. In the large- N calculation based on Eq. (10), we find that both states can be stabilized in the presence of Kondo screening. The P_L -CSL state emerges as the ground state first, but the $P_L - \pi$ -flux state eventually takes over at larger J_K/J_1 (see Fig. (S5) and related Supplemental Material for details).

For the π -flux phase, $H_{QSL} = H_{\pi\text{-flux}}$ is given by $A_{\mathbf{r}_i, \mathbf{r}_i + \hat{x}} = \pi/2$, $A_{\mathbf{r}_i, \mathbf{r}_i + \hat{y}} = -(-1)^{x_i} \pi/2$, $\rho_{\mathbf{r}_i, \mathbf{r}_i + \hat{x} + \hat{y}} = 0$, where $\mathbf{r}_i = (x_i, y_i)$, \hat{x} (\hat{y}) is the unit vector along the x (y)-axis. For the CSL Hamiltonian, $H_{QSL} = H_{\text{CSL}}$ is derived from $H_{\pi\text{-flux}}$ with $\rho_{\mathbf{r}_i, \mathbf{r}_i + \hat{x} + \hat{y}} \neq 0$, $A_{\mathbf{r}_i, \mathbf{r}_i + \hat{x} + \hat{y}} = A_{\mathbf{r}_i + \hat{y}, \mathbf{r}_i + \hat{x}} = (-1)^{x_i} \pi/2$, as illustrated in Fig. (1c).

In the kagomé lattice, any state with triangle flux $\phi \neq 0, \pi$ breaks TRS. Here, we choose $\phi = -\frac{\pi}{2}$ such that the hexagon flux of $-2\phi = \pi$ preserves TRS. The $(-\frac{\pi}{2}, \pi)$ spinon flux state has three well-separated bands; the middle flat band is exactly at the Fermi energy, and the Chern numbers are $C_{\text{lower}} = -1$, $C_{\text{middle}} = 0$, $C_{\text{upper}} = +1$ [39]. These band structures can be considered as the usual, no-flux kagomé bands inverted by the fluxes. The phase structure of the corresponding χ_{ij} fields is plotted in Fig. (1d).

The zero-field anomalous Hall conductivity σ_{xy} of the $J_1 - J_2 - J_K$ model is shown in Fig. (2a) for representative parameters $n_d = 0.5$, $J_1 = t$ and that of the kagomé lattice model in Fig (2b) for $J = t$, $n_d = 3/8$. Across the QCP, σ_{xy} is found *continuous* for the square lattice, but *jumps discontinuously* for the kagomé lattice. The amplitudes of σ_{xy} are similar in the P_S regimes, $\sim 10^{-2} \sigma_0$. But σ_{xy} is enhanced by two orders of magnitude in the P_L regime of the kagomé case.

In order to understand the different behaviors, we show the Fermi surfaces (dashed lines) and the difference of band-summed Berry curvature $\Delta\Omega(\mathbf{k})$ (color map) between the P_S phase and the P_L phase right across the

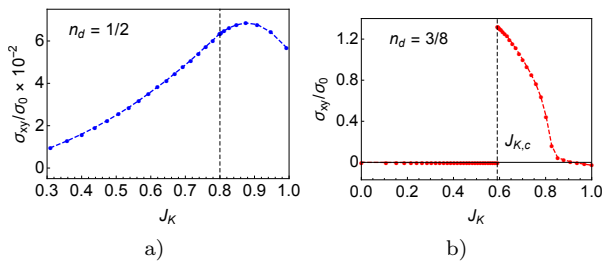


FIG. 2. (Color online) Zero field anomalous Hall conductance (σ_{xy}), normalized by the quantum conductance $\sigma_0 = e^2/h$, for $J_1 = t = 1$, $J_2/J_1 = 1/2$, $n_d = 0.5$ on a square lattice (a) and for $J = t$, $n_d = 3/8$ on a Kagomé lattice (b).

QCP in Fig. (3a) for the square lattice and (3b) for the kagomé lattice (the actual $\Omega(\mathbf{k})$ is shown in Supplemental Material). Here $\Delta\Omega(\mathbf{k}) = \Omega_{P_S}(\mathbf{k}) - \Omega_{P_L}(\mathbf{k})$ and $\Omega(\mathbf{k}) = \sum_n \mathcal{F}_n^{xy}(\mathbf{k}) f(\epsilon_n(\mathbf{k}))$. We find the Fermi surfaces remain continuous for the square lattice model. Both Fermi surfaces of the P_S and P_L phases are the black dashed line. However, for the kagomé case, the Fermi surfaces show a jump. The Fermi surface of the P_S phase is the black dashed circle in the middle of the BZ which overlaps with the red, singular part of $\Delta\Omega(\mathbf{k})$. Those of the P_L phase are the blue dashed-line pockets at the edge of the BZ. These results reflect the number of sites per unit cell and the gapped/gapless nature of the spinon spectrum. However, $\Delta\Omega(\mathbf{k})$ is singular and concentrates near Fermi surfaces in both cases. This is because the onset of Kondo hybridization, which acts as a topological mass term in the large- N theory, in general singularly reconstructs the wavefunctions regardless of whether the Fermi surfaces jump or not.

To reconcile the notions of the singular wavefunction (or Berry curvature) with the continuous AHE, we note that σ_{xy} is intrinsically a Fermi surface property [27] (apart from the contributions of fully occupied bands). We can analytically show the following by computing the diagonal Berry's connection in the $\rho_K \rightarrow 0$ limit [32]. When the Fermi surfaces evolve continuously across the QCP, σ_{xy} must be continuous; here, the projected wavefunctions of the d -electron are continuous, and so are the Berry connections. By contrast, when the Fermi surface jumps, the projected wavefunctions completely reconstruct due to the existence of two non-commuting topological “masses”: the Kondo screening and a non-zero jump of the spinon Lagrangian multiplier λ .

Discussion. Energetic considerations[40] show that the Kondo coupling favors gapless states (Supplemental Material [32]), since the formation of a Kondo singlet generally needs to overcome the spinon gap, if any, lowering the energy by an amount $\propto J_K$. For the pyrochlore lattice, the CSL state in the large- N limit is gapless [41], and is thus expected to have a similar sequence of quantum phase transitions involving the chiral state. The gapless

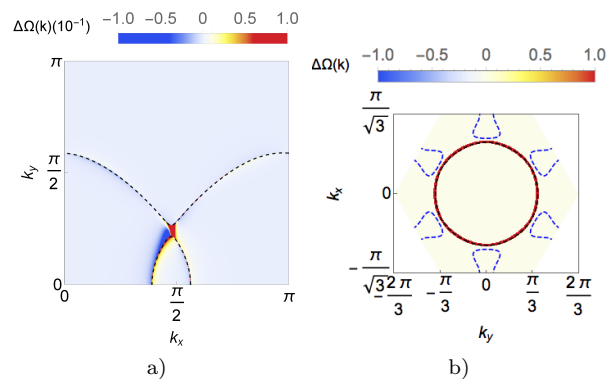


FIG. 3. (Color online) Fermi surfaces (dashed curves) and the difference in the band-summed Berry curvature distribution $\Delta\Omega(\mathbf{k})$ between the P_S phase and the P_L phase (color map) of the square lattice model (3a) and the kagomé lattice model (3b).

nature raises the prospect of a sudden reconstruction of the Fermi surface across a Kondo-destruction QCP in the pyrochlore case and, by extension, a jump in the zero-field AHE, especially for a magnetic field along the [111] direction.

We expect the jump of the zero field AHE, σ_{xy} , to be robust against weak disorder. The AHE effect considered here is intrinsic, i.e., determined by the quasi-particle band structure. Scattering from weak non-magnetic impurities only yields a small (linear in disorder) correction [43]. Moreover, the Fermi-surface jump across a Kondo-destruction QCP has been evidenced to be robust against weak disorder [12, 42]. Thus, our results can be tested in $\text{Pr}_2\text{Ir}_2\text{O}_7$, once a control parameter is identified to tune across the implicated zero-field QCP [25]. From Ref. 44, strain can potentially serve as such a tuning parameter.

We note that the anomalous Hall conductance from the mechanism advanced here is quite large. Experiments in $\text{Pr}_2\text{Ir}_2\text{O}_7$ [16] find a large sheet σ_{xy} reaching about 0.7% of $\sigma_0 \equiv e^2/h$, a value which readily arise in our mechanism (Fig. 2a).

We have emphasized the role of the Kondo effect and its critical destruction. Future work should incorporate *ab initio* features, not only on the directional dependence in the pyrochlore lattice but also the effect of the *ab initio* electronic band structure and the non-Kramers nature of the ground-state crystal-field level of the Pr ions [24, 45]. Although Ref. [24] studied a realistic model, the mechanism of AHE in the Kondo destroyed phase is not captured, and σ_{xy}^{AHE} only starts to grow from zero at the QCP. The new mechanism we consider here provides a possible interpretation to the experimental observation that σ_{xy}^{AHE} is most singular at the QCP.

Furthermore, we have derived our conclusions in geometrically frustrated Kondo systems and demonstrated the robustness of our results by connecting them with

the evolution of the Fermi surfaces. Thus, we expect our results to remain qualitatively valid in the more realistic settings. For $\text{Pr}_2\text{Ir}_2\text{O}_7$, this is so given the substantial evidence for the role of the Kondo coupling such as the large entropy observed in the pertinent low-temperature regime [25]. It may also be instructive to explore related effects in other f -electron systems with geometrical frustration, such as UCu_5 under ambient conditions[46] and when suitably tuned through a QCP. Recently, the proximity to the Kondo-destruction QCP we predict here for $\text{Pr}_2\text{Ir}_2\text{O}_7$ is confirmed experimentally[47]. In this STM measurement, regions of heavy Fermi liquid are interwoven with a non-magnetic metallic phase with Kondo-destruction, forming spatial nanoscale patterns consistent with being in proximity to a critical point.

While the current work emphasizes the link between AHE and the evolution of Fermi surfaces due to Kondo physics, other topology-related components, such as conduction band topology, k -dependence of Kondo coupling, etc., are not taken into account. It is known that such components can lead to topological Kondo lattice models that realize such topological states as Weyl-Kondo semimetals [48–51]. In addition, d -electron-based systems on frustrated lattices, through the notion of compact molecular orbitals, can realize topological Kondo lattice models and the associated states [52–54]. For these states, Berry-curvature-induced Hall effect is also an important characteristic; thus, we expect our work here will provide new insights into those systems.

We close by proposing an engineered Kondo-insulator interface as a model material for the frustrated Kondo lattice Hamiltonian. The motivation for the proposed setting comes from advances in the molecular beam epitaxy (MBE) of Kondo systems [55–57]. As a promising candidate material, we suggest the golden phase of SmS (g -SmS). In bulk samples, this phase is stable under pressures between about 0.65 GPa [58] and 2 GPa [59]. As MBE thin-film, the phase might be stabilized by lattice mismatch with an appropriate substrate. g -SmS crystallizes in a face-centered-cubic (fcc) structure of rock-salt (NaCl) type. A lattice plane is shown in Fig. (S6). g -SmS shows characteristics of a Kondo insulating state in transport [59, 60], thermodynamics [61], and point contact spectroscopy [60]. From thermal expansion and heat capacity measurements, the energy gap was estimated to be 90 K on the low-pressure side of the g -SmS phase [61]. At temperatures low compared to this scale, the proposed lattice plane could then serve as a setting to realize the frustrated $J_1 - J_2$ Kondo lattice and study the anomalous Hall effect.

Note added: Since our manuscript was posted, chiral heavy fermion phase and its associated Kondo-destruction transition have also been discussed in the context of moiré structures of transition metal dichalcogenides [62, 63].

We acknowledge useful discussions with P. Gegenwart,

S. Nakatsuji and P. Goswami. Work at Rice University has primarily been supported by the National Science Foundation under Grant No. DMR-2220603 (model conceptualization, W.D. and S.E.G.), by the Air Force Office of Scientific Research under Grant No. FA9550-21-1-0356 (model calculations, W.D. and S.E.G.), by the Robert A. Welch Foundation Grant No. C-1411 and the Vannevar Bush Faculty Fellowship ONR-VB N00014-23-1-2870 (conceptualization, Q.S.). Work at Anhui University was supported by the National Key R&D Program of the MOST of China under Grant No. 2022YFA1602603 (W.D.).

† These two authors contributed equally to this work.

-
- [1] P. Coleman and A. J. Schofield, *Nature* **433**, 226 (2005).
 - [2] H. Hu, L. Chen, and Q. Si, *Nat. Phys.*, to appear, arXiv:2210.14183.
 - [3] S. Kirchner, S. Paschen, Q. Chen, S. Wirth, D. Feng, J. D. Thompson, and Q. Si, *Reviews of Modern Physics* **92**, 011002 (2020).
 - [4] Q. Si, *Physica B* **378**, 23 (2006); Q. Si, *Phys. Status Solidi B* **247**, 476 (2010).
 - [5] P. Coleman and A. H. Nevidomskyy, *J. Low Temp. Phys.* **161**, 182 (2010).
 - [6] Q. Si, S. Rabello, K. Ingersent, and J. L. Smith, *Nature* **413**, 804 (2001).
 - [7] M. S. Kim and M. C. Aronson, *Phys. Rev. Lett.* **110**, 017201 (2013).
 - [8] E. D. Mun, S. L. Bud'ko, C. Martin, H. Kim, M. A. Tanatar, J.-H. Park, T. Murphy, G. M. Schmiedeshoff, N. Dilley, R. Prozorov, and P. C. Canfield, *Phys. Rev. B* **87**, 075120 (2013).
 - [9] V. Fritsch, N. Bagrets, G. Goll, W. Kittler, M. J. Wolf, K. Grube, C.-L. L. Huang, and H. V. Löhneysen, *Phys. Rev. B* **89**, 054416 (2014).
 - [10] Y. Tokiwa, C. Stingl, M.-S. Kim, T. Takabatake, and P. Gegenwart, *Sci. Adv.* **1**, e1500001 (2015).
 - [11] S. Nakatsuji, Y. Machida, Y. Maeno, T. Tayama, T. Sakakibara, J. Duijn, L. Balicas, J. Millican, R. Macaluso, and J.Y. Chan, *Phys. Rev. Lett.* **96**, 087204 (2006).
 - [12] Q. Si and S. Paschen, *Phys. Status Solidi B* **250**, 425 (2013).
 - [13] H. Zhao, J. Zhang, M. Lyu, S. Bachus, Y. Tokiwa, P. Gegenwart, S. Zhang, J. Cheng, Y. feng Yang, G. Chen, Y. Isikawa, Q. Si, F. Steglich, and P. Sun, *Nat. Phys.* **15**, 1261 (2019).
 - [14] S. Paschen and Q. Si, *Nat. Rev. Phys.* **3**, 9 (2021).
 - [15] Y. Machida, S. Nakatsuji, Y. Maeno, T. Tayama, T. Sakakibara, and S. Onoda, *Phys. Rev. Lett.* **98**, 057203 (2007).
 - [16] Y. Machida, S. Nakatsuji, S. Onoda, T. Tayama, and T. Sakakibara, *Nature* **463**, 210 (2010).
 - [17] G. Chen and M. Hermele, *Phys. Rev. B* **86**, 235129 (2012).
 - [18] R. Flint and T. Senthil, *Phys. Rev. B* **87**, 125147 (2013).
 - [19] S.B. Lee, A. Paramekanti, and Y. B. Kim, *Phys. Rev. Lett.* **111**, 196601 (2013).
 - [20] E.-G. Moon, C. Xu, Y. B. Kim, and L. Balents, *Phys.*

- Rev. Lett. **111**, 206401 (2013).
- [21] L. Savary, E.-G. Moon, and L. Balents, Phys. Rev. X **4**, 041027 (2014).
- [22] M. Udagawa and R. Moessner, Phys. Rev. Lett. **111**, 036602 (2013).
- [23] A. Kalitsov, B. Canals, and C. Lacroix, J. Phys. Conf. Ser. **145**, 012020 (2009).
- [24] J. G. Rau and H.-Y. Kee, Phys. Rev. B **89**, 075128 (2014).
- [25] Y. Tokiwa, J. J. Ishikawa, S. Nakatsuji, and P. Gegenwart, Nat. Mater. **13**, 356 (2014).
- [6] S. Paschen, T. Lühmann, S. Wirth, P. Gegenwart, O. Trovarelli, C. Geibel, F. Steglich, P. Coleman, and Q. Si, Nature **432**, 881 (2004).
- [27] F. D. M. Haldane, Phys. Rev. Lett. **93**, 206602 (2004).
- [28] X.G. Wen, F. Wilczek, and A. Zee, Phys. Rev. B **39**, 11413 (1989).
- [29] Y.-C. He, D. N. Sheng, and Y. Chen, Phys. Rev. Lett. **112**, 137202 (2014), S.-S. Gong, W. Zhu, and D. N. Sheng, Sci. Rep. **4**, 6317 (2014).
- [30] S. Bieri, L. Messio, B. Bernu, and C. Lhuillier, Phys. Rev. B **92**, 060407 (2015).
- [31] I. Affleck and J.B. Marston, Phys. Rev. B **37**, 3774 (1988).
- [32] See Supplemental Material, which includes Refs.[1–3, 5, 7], for a discussion of the six-fermion chiral interactions for both the P_S and P_L phases, the special form of a Hubbard-Stratonovich transformation for the chiral interactions, the Streda and Kubo formulae for the calculation of the Hall conductivity, the reconstruction of the Fermi surfaces and wavefunctions across the QCP, the saddlepoint analysis for the phase diagram, and a proposal for additional materials realization.
- [1] S. Florens and A. Georges, Phys. Rev. B **70**, 035114 (2004).
- [2] S. Florens and A. Georges, Phys. Rev. B **66**, 165111 (2002).
- [3] W. Ding, R. Yu, Q. Si, and E. Abrahams, Phys. Rev. B **100**, 235113 (2019).
- [5] K. Sun and E. Fradkin, Phys. Rev. B **78**, 245122 (2008).
- [7] M. Oshikawa, Phys. Rev. Lett. **84**, 3370 (2000).
- [38] P. Streda, J. Phys. C Solid State Phys. **15**, L717 (1982).
- [39] N. Nagaosa, S. Onoda, A. H. MacDonald, and N. P. Ong, Rev. Mod. Phys. **82**, 1539 (2010).
- [40] P. Coleman and N. Andrei, J. Phys. Condens. Matter **4057**, 4057 (1989).
- [41] F. J. Burnell, S. Chakravarty, and S. L. Sondhi, Phys. Rev. B **79**, 144432 (2008).
- [42] P. Gegenwart, Q. Si, and F. Steglich, Nat. Phys. **4**, 186 (2008).
- [43] N. Sinitsyn, a. MacDonald, T. Jungwirth, V. Dugaev, and J. Sinova, Phys. Rev. B **75**, 045315 (2007).
- [44] T. Ohtsuki, Z. Tian, A. Endo, M. Halim, S. Katsumoto, Y. Kohama, K. Kindo, M. Lippmaa, and S. Nakatsuji, Proc. Natl. Acad. Sci. **116**, 8803 (2019).
- [45] P. Chandra, P. Coleman, and R. Flint, Nature **493**, 621 (2013).
- [46] B. Ueland, C. Miclea, Y. Kato, O. Ayala-Valenzuela, R. McDonald, R. Okazaki, P. Tobash, M. Torrez, F. Ronning, R. Movshovich, Z. Fisk, E. Bauer, I. Martin, and J. Thompson, Nat. Commun. **3**, 1067 (2012).
- [47] M. Kawai, J. Friedman, K. Sherman, M. Gong, I. Giannakis, S. Hajinazar, H. Hu, S. E. Grefe, J. Leshen, Q. Yang, S. Nakatsuji, A. N. Kolmogorov, Q. Si, M. Lawler, and P. Aynajian, Nat. Commun. **12**, 1377 (2021).
- [48] H.-H. Lai, S. E. Grefe, S. Paschen, and Q. Si, Proc. Natl. Acad. Sci. **115**, 93 (2017).
- [49] L. Chen, C. Setty, H. Hu, M. G. Vergniory, S. E. Grefe, L. Fischer, X. Yan, G. Eguchi, A. Prokofiev, S. Paschen, J. Cano, and Q. Si, Nat. Phys. **18**, 1341 (2022).
- [50] S. Dzsaber, L. Prochaska, A. Sidorenko, G. Eguchi, R. Svagera, M. Waas, A. Prokofiev, Q. Si, and S. Paschen, Phys. Rev. Lett. **118**, 246601 (2017).
- [51] S. Dzsaber, X. Yan, M. Taupin, G. Eguchi, A. Prokofiev, T. Shiroka, P. Blaha, O. Rubel, S. E. Grefe, H.-H. Lai, Q. Si, and S. Paschen, Proc. Natl. Acad. Sci. **118**, e2013386118 (2021).
- [52] L. Chen, F. Xie, S. Sur, H. Hu, S. Paschen, J. Cano, and Q. Si, arXiv:2307.09431.
- [53] L. Chen, F. Xie, S. Sur, H. Hu, S. Paschen, J. Cano, and Q. Si, Nat. Comm. **15**, 5242 (2024).
- [54] H. Hu and Q. Si, Sci. Adv. **9**, eadg0028 (2023).
- [55] H. Shishido, T. Shibauchi, K. Yasu, T. Kato, H. Kontani, T. Terashima, and Y. Matsuda, Science **327**, 980 (2010).
- [56] S. K. Goh, Y. Mizukami, H. Shishido, D. Watanabe, S. Yasumoto, M. Shimozawa, M. Yamashita, T. Terashima, Y. Yanase, T. Shibauchi, a. I. Buzdin, and Y. Matsuda, Phys. Rev. Lett. **109**, 157006 (2012).
- [57] L. Prochaska, X. Li, D. C. MacFarland, A. M. Andrews, M. Bonta, E. F. Bianco, S. Yazdi, W. Schrenk, H. Detz, A. Limbeck, Q. Si, E. Ringe, G. Strasser, J. Kono, and S. Paschen, Science **367**, 285 (2020).
- [58] M. B. Maple and D. Wohlleben, Phys. Rev. Lett. **27**, 511 (1971).
- [59] Y. Haga, J. Derr, a. Barla, B. Salce, G. Lapertot, I. Sheikin, K. Matsubayashi, N. K. Sato, and J. Flouquet, Phys. Rev. B **70**, 220406 (2004).
- [60] P. Wachter, in *Handbook of the Physics and Chemistry of Rare Earths*, edited by K. A. Gschneidner Jr., L. Eyring, and S. Hüfner (North-Holland, Amsterdam, 1994), pp. 177, Vol. 19.
- [61] K. Matsubayashi, K. Imura, H. S. Suzuki, G. Chen, N. Mori, T. Nishioka, K. Deguchi, and N. K. Sato, J. Phys. Soc. Japan **76**, 033602 (2007).
- [62] A. Kumar, N. C. Hu, A. H. MacDonald, and A. C. Potter, Phys. Rev. B **106**, L041116 (2022).
- [63] D. Guerci, J. Wang, J. Zang, J. Cano, J. H. Pixley, and A. Millis, Sci. Adv. **9**, nil (2023).

Supplemental Materials

Chiral interaction from perturbative expansion

H_{chiral} of the Kondo destroyed P_S Phase. To obtain Eq. (5) of the main text, we integrate out the f -spinons from Eqs. (1,2) of the main text in the Kondo destroyed phase using the standard Feynman diagram procedure. Guided by symmetry analysis, we only need to consider the third-order term $1/3!(\mathbf{s}_i \cdot \mathbf{S}_i)(\mathbf{s}_j \cdot \mathbf{S}_j)(\mathbf{s}_k \cdot \mathbf{S}_k)$. The effective chiral electronic interaction H_{cc} is obtained by contracting the spinons in triangle-loop diagrams as shown Fig. (S1).

Since the CSL is gapped, it is sufficient to restrict to the most local three-site loops, i.e., the triangle within a unit cell, at equal time only. Then we can obtain H_{chiral} as follows:

$$\begin{aligned} (\mathbf{s}_i \cdot \mathbf{S}_i)(\mathbf{s}_j \cdot \mathbf{S}_j)(\mathbf{s}_k \cdot \mathbf{S}_k) &= \sum_{a,b,c} s_i^a s_j^b s_k^c \\ &\times \frac{1}{8} (f_{i\alpha_i}^\dagger \sigma_{\alpha_i\beta_i}^a f_{i\beta_i} f_{j\alpha_j}^\dagger \sigma_{\alpha_j\beta_j}^b f_{j\beta_j} f_{k\alpha_k}^\dagger \sigma_{\alpha_k\beta_k}^c f_{k\beta_k}) \\ &\xrightarrow{\Delta} \sum_{a,b,c} s_i^a s_j^b s_k^c (\langle f_{i\alpha_i}^\dagger f_{j\beta_j} \rangle \langle f_{j\alpha_j}^\dagger f_{k\beta_k} \rangle \langle f_{k\alpha_k}^\dagger f_{i\beta_i} \rangle) \\ &+ \langle f_{i\alpha_i}^\dagger f_{k\beta_k} \rangle \langle f_{k\alpha_k}^\dagger f_{j\beta_j} \rangle \langle f_{j\alpha_j}^\dagger f_{i\beta_i} \rangle \sigma_{\alpha_i\beta_i}^a \sigma_{\alpha_j\beta_j}^b \sigma_{\alpha_k\beta_k}^c \\ &= E_{ijk} \mathbf{s}_i \cdot (\mathbf{s}_j \times \mathbf{s}_k) / 2, \end{aligned} \quad (\text{S-1})$$

where Δ denotes the triangular-loop contraction. The contraction is approximated by equal-time correlators, so $\langle f_{i\alpha_i}^\dagger f_{j\beta_j} \rangle = \delta_{\alpha_i, \beta_j} \chi_{ij}$. To isolate the chiral processes, we can discard the density-density interactions. As a result, the second line of Eq. (S-1) can be written as

$$\begin{aligned} H_{\text{chiral}} \sim &\sum_{\alpha_l, \alpha_j, \alpha_k} (P_{ljk} d_{l\alpha_k}^\dagger d_{l\alpha_l} d_{j\alpha_l}^\dagger d_{j\alpha_j} d_{k\alpha_j}^\dagger d_{k\alpha_k}) \\ &+ P_{lkj} d_{l\alpha_j}^\dagger d_{l\alpha_l} d_{k\alpha_l}^\dagger d_{k\alpha_k} d_{j\alpha_k}^\dagger d_{j\alpha_j}). \end{aligned} \quad (\text{S-2})$$

H_{chiral} of the Kondo Screened P_L Phase. To obtain the spectral weight of the incoherent terms in the Kondo screened phase, we use the slave rotor theory[1] to tackle the f -fermion Hubbard model. As we shall briefly discuss below, the Kondo transition is the Mott transition for f -fermions in periodic Anderson model (PAM)[2], and is realized when the rotor fields are condensed. The condensation density describes the coherent charge degrees of freedom that would contribute to transport.

The PAM Hamiltonian is

$$H_{\text{PAM}} = H_{\text{Hubbard}}^{(f')} + H_0^{(d)} + V \sum_{i,\sigma} (f_{i,\sigma}^\dagger d_{i,\sigma} + f_{i,\sigma}' d_{i,\sigma}^\dagger), \quad (\text{S-3})$$

where

$$H_{\text{Hubbard}}^{(f')} = - \sum_{ij,\sigma} t_{ij} f_{i,\sigma}^\dagger f_{j,\sigma}' + U \sum_{i,\sigma,\sigma'} n_{i,\sigma}^{(f')} n_{i,\sigma'}^{(f')} \quad (\text{S-4})$$

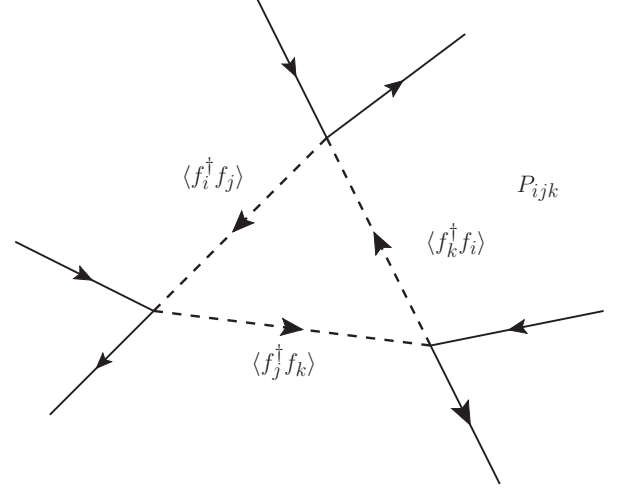


FIG. S1. Feynman diagrams of the triangle-loop contractions. The solid lines are the propagators for the conduction electrons, and the dashed lines for the spinons.

is the usual half-filled Hubbard model, and

$$H_0^{(d)} = - \sum_{ij,\sigma} t_{ij} d_{i,\sigma}^\dagger d_{j,\sigma} \quad (\text{S-5})$$

describes the free d -band electrons.

First, we use the slave rotor formalism to treat the Hubbard model part by letting $f_i' \rightarrow f_i e^{-i\theta_i}$

$$H^{(f')} \rightarrow \frac{U}{2} \sum_{i,\sigma} \hat{L}_{i,\sigma}^2 - \sum_{ij,\sigma} (t_{ij} f_{i,\sigma}^\dagger f_{j,\sigma} e^{i(\theta_i - \theta_j)} + h.c.). \quad (\text{S-6})$$

The corresponding Lagrangian is

$$\begin{aligned} S_H = &\int d\tau \sum_{i,\sigma} f_{i,\sigma}^\dagger \partial_\tau f_{i,\sigma} + \frac{(\partial_\tau \theta)^2}{2U} + \\ &\sum_{\langle ij \rangle, \sigma} (t_{\langle ij \rangle} f_{i,\sigma}^\dagger f_{j,\sigma} e^{i(\theta_i - \theta_j)} + h.c.), \end{aligned} \quad (\text{S-7})$$

here the kinetic energy of the rotors $\frac{U}{2} \sum_{i,\sigma} \hat{L}_{i,\sigma}^2$ is replaced by its conjugate variables $\hat{L}_{i,\sigma} = (\partial_\tau \theta + ih)/U$.

Let $e^{i\theta_i} = X_i$, so that X_i s subject to the constraint $|X_i|^2 = 1$ on average (using Lagrangian multiplier). Using $\partial_\tau \theta_i = \frac{1}{i} X_i^* \partial_\tau X_i$, we have

$$S_H = S_X^0 + S_f^0 + \sum_{\langle ij \rangle, \sigma} (t_{\langle ij \rangle} f_{i,\sigma}^\dagger f_{j,\sigma} X_i X_j^* + h.c.). \quad (\text{S-8})$$

with $S_f^0 = \int d\tau \sum_{i,\sigma} f_{i,\sigma}^\dagger \partial_\tau f_{i,\sigma}$, and $S_X^0 = \sum_i (\frac{|\partial_\tau X_i|^2}{2U} + \lambda_i (|X_i|^2 - 1))$. The exchange term is also expressed in

terms of slave rotors

$$H_{\text{exc}} = V \sum_{i,\sigma} (f_{i,\sigma}^\dagger d_{i,\sigma} X_i + h.c.). \quad (\text{S-9})$$

In the large- U -small- V limit, the system is in P_S phase. We can integrate out the rotor fields[3], and recover both the Heisenberg- J interaction, as well as the Kondo coupling

$$H_K = J_K \sum_i \mathbf{S}_f(i) \cdot \mathbf{s}_d(i), \quad (\text{S-10})$$

where $J_K = 4V^2/U$.

Within the slave rotor approach, the onset of Kondo screening is described by the condensation of the X -field: $X_i \rightarrow X_i^0 + X_i'$. The exchange term becomes

$$H_{\text{exc}} = \sum_{i,\sigma} (V X_i^0 f_{i,\sigma}^\dagger d_{i,\sigma} + V X_i' f_{i,\sigma}^\dagger d_{i,\sigma} + h.c.). \quad (\text{S-11})$$

The first term is the hybridization term, which is equivalent to that of the Kondo model. We can identify that $\rho_K = V X_i^0 / J_K = \frac{U}{4V} X_i^0$. The second term now provides the incoherent fluctuations, which, as we argue in the main text, can mediate the same chiral interactions for the d -electrons through the triangular diagrams. But in this approach, the X -field satisfies a spectral sum rule: $\int d\nu d^2k / (2\pi)^3 G_X(\nu; \mathbf{k}) = 1$, from which we can obtain that in the Kondo screened phase

$$H_{\text{chiral}} = \left(1 - \frac{4J_K}{U} \rho_K^2\right)^3 \frac{J_K^3}{2} E_{ijk} \mathbf{s}_i \cdot (\mathbf{s}_j \times \mathbf{s}_k). \quad (\text{S-12})$$

Note that the prefactor $4J_K/U$ is changing as we tune J_K . In our calculation, we fix $U = 16t$, i.e. twice as the d -electron's bandwidth.

Hubbard-Stratonovich transformation of H_{chiral} . In this part, we construct a Hubbard-Stratonovich (HS) transformation to decouple the six-fermion chiral interaction of Eq. (S-12). With such a HS transformation, we apply a gauge fixing condition so that the time-reversal-symmetry breaking phases are carried by the fermion bilinears, which yields Eq. (8) of the main text.

In general, we need to introduce two sets of Hubbard-Stratonovich (HS) fields, namely, γ_s, κ_s , which can be interpreted as a single bond / two consecutive bonds fields:

$$\gamma_{ij} = \langle \sum_\alpha d_{i,\alpha}^\dagger d_{j,\alpha} \rangle, \quad (\text{S-13})$$

$$\kappa_{ij,k} = \langle \sum_{\alpha,\beta} d_{i,\alpha}^\dagger d_{k,\alpha} d_{j,\beta}^\dagger d_{j,\beta} \rangle, \quad (\text{S-14})$$

which are, in principle, independent. The bond indices here are directional, i.e. $\gamma_{ji} = \gamma_{ij}^*$, $\kappa_{ji,k} = \kappa_{ij,k}^*$. There are 6 complex γ 's and 12 complex κ 's.

The HS transformation is as follows

$$L_{\text{HS}} = \sum_{\mathbf{x}} (d_{\mathbf{x}}^\dagger (i\partial_t + \mu) d_{\mathbf{x}} - \tilde{\Psi}^* \mathcal{M} \Psi + J^\dagger \Psi + \tilde{\Psi}^* J - H_{\text{kin}}), \quad (\text{S-15})$$

where $\tilde{\Psi}^* = \{\kappa_{\mathbf{x}_i \mathbf{x}_j, k}^*, \dots, \kappa_{\mathbf{x}_i \mathbf{x}_j, \bar{k}}^*, \dots, \gamma_{\mathbf{x}_i \mathbf{x}_j}, \dots, \gamma_{\mathbf{x}_j \mathbf{x}_i}, \dots\}$ is a 24-component vector. The indices $i - j$ run over all the links inside a unit cell given by \mathbf{x} , and $\{k, \bar{k}\}$ denote the other two sites for a given bond $\langle ij \rangle$ within the unit cell.

$$J^\dagger = \{\hat{\gamma}_{ij}^\dagger, \hat{\gamma}_{ji}^\dagger, \dots, \hat{\kappa}_{ij,k}^\dagger, \hat{\kappa}_{ij,\bar{k}}^\dagger, \dots\}. \quad (\text{S-16})$$

where we use $\hat{\gamma}_{ij}^\dagger = \sum_\alpha d_{\mathbf{x}_j, \alpha}^\dagger d_{\mathbf{x}_i, \alpha}$, $\hat{\kappa}_{ij,k}^\dagger = \sum_{\alpha,\beta} d_{j,\alpha}^\dagger d_{k,\alpha} d_{k,\beta}^\dagger d_{i,\beta}$.

To determine \mathcal{M} , suppose that we now integrate out all the HS fields, we should recover the effective interactions as

$$H_{\text{eff-int}} = J^\dagger \mathcal{M}^{-1} J = H_{\text{cc}} + \dots, \quad (\text{S-17})$$

in which the \dots indicates other effective interactions. To have a stable HS transformation, we need to include further the 4-fermion effective interactions at $H_{\text{eff-int}}^{(2)} \sim \mathcal{O}(J_K^2)$ generated from $J_K^2 (\mathbf{s}_i \cdot \mathbf{S}_i) (\mathbf{s}_j \cdot \mathbf{S}_j)$ as well as the 8-fermion process at $H_{\text{eff-int}}^{(4)} \sim \mathcal{O}(J_K^4)$. Since the f -fermions are gapped, we can keep only the short-range terms, i.e. within a unit cell, so that all the terms can be decoupled by the $\hat{\gamma}_{ij}$ s and $\hat{\kappa}_{ij}$ s in the large- N limit. Then \mathcal{M}^{-1} can be written in a block form $\mathcal{M}^{-1} = \oplus (\mathcal{M}_{(ij)}^{-1})$, where $(\mathcal{M}_{(ij)}^{-1})$ is a 4×4 matrix for a given bond (ij) within the unit cell.

Here we estimate the matrix elements of $(\mathcal{M}_{(ij)}^{-1})$ within the approximations that are used for computing H_{chiral} , i.e., equal-time contraction is used and only those within a unit cell are included:

$$(M^{-1})_{\hat{\gamma}^\dagger \hat{\gamma}, (ij)} = J_K^2 \text{sgn}[(ij)] \chi_{ij} \chi_{ji} / 2! = \rho_{ij}^2, \quad (\text{S-18})$$

$$(M^{-1})_{\hat{\kappa} \hat{\gamma}, (ij)k} = J_K^3 P_{ijk} / (2 \times 3!), \quad (\text{S-19})$$

$$(M^{-1})_{\hat{\kappa}^\dagger \hat{\kappa}, (ij), kk'} = \delta_{k,k'} J_K^4 \rho_{ij}^4 / 4!. \quad (\text{S-20})$$

$\text{sgn}[(ij)]$ is a relative sign coming from the fact that $\hat{\gamma}_{ij}^\dagger \hat{\gamma}_{ij} \sim -\hat{\gamma}_{ji}^\dagger \hat{\gamma}_{ji}$. We see that $\det[\mathcal{M}^{-1}]$ is indeed positive; hence, this is a stable HS transformation. \mathcal{M} is then obtained by inverting \mathcal{M}^{-1} .

Therefore, we have a formal HS decoupling of H_{chiral} . Further replacing the HS-fields by their expectation values in Eq. (S-15), we obtain both fermion bilinears and four-fermion terms. To lower the total energy, we need to have $\gamma_{ij} \kappa_{ij,k}^* \sim -P_{ijk}$. Upon satisfying this constraint, we have an additional gauge degree of freedom to choose either $\gamma_{d,ij}$ or $\kappa_{ij,k}^*$ to be imaginary, i.e. explicitly breaking TRS, even though the underlying physical state is the same. For convenience, we can choose $\kappa_{ij,k}^*$ s which couple to d -fermion bilinears ($\hat{\gamma}_{ij}$ s) to be TRSB. By keeping only the TRSB terms in Eq. (S-15), we justify our choice of Eq. (8) in the main text as

$$H_{d,1} = \sum_{\langle ij \rangle, k} (\kappa_{ij,k}^* \hat{\gamma}_{ij} + h.c.). \quad (\text{S-21})$$

Berry curvature, Berry connection, Streda formula and Kubo formula

The AHE coefficient, σ_{xy} , presented in the main text are computed using the Streda formula:

$$\begin{aligned}\sigma_{xy} &= \int \frac{d\mathbf{k}}{(2\pi)^2} \sum_n \mathcal{F}_n^{xy}(\mathbf{k}) f(\epsilon_n(\mathbf{k})) \\ &= \sum_{n \neq n'} \int \frac{d\mathbf{k}}{(2\pi)^2} [f(\epsilon_n(\mathbf{k})) - f(\epsilon_{n'}(\mathbf{k}))] \\ &\quad \times \text{Im} \frac{\langle n, \mathbf{k} | v_x(\mathbf{k}) | n', \mathbf{k} \rangle \langle n', \mathbf{k} | v_y(\mathbf{k}) | n, \mathbf{k} \rangle}{[\epsilon_n(\mathbf{k}) - \epsilon_{n'}(\mathbf{k})]^2}.\end{aligned}\quad (\text{S-22})$$

Here, $v_a(\mathbf{k}) = \partial_a H_d(\mathbf{k})$ is the current operator of the conduction electrons, $\mathcal{F}_n^{xy}(\mathbf{k})$ the Berry curvature, and $f(\epsilon_n(\mathbf{k}))$ the Fermi function. Both \hbar and e have been taken to be 1.

To discuss the role of the Berry curvature, we start from the more standard Kubo formula. The current operators are

$$\mathbf{J}_q = \frac{1}{\sqrt{N}} \sum_{\mathbf{k}} c_{\mathbf{k}+\mathbf{q}/2}^\dagger \frac{\partial H_{\mathbf{k}}}{\partial \mathbf{k}} c_{\mathbf{k}-\mathbf{q}/2}. \quad (\text{S-23})$$

In frequency-momentum space, the conductivity is computed via the current-current correlation function

$$\begin{aligned}\pi_{ab}(i\nu) &= \sum_{\omega} \int \frac{d^2k}{(2\pi)^2} \text{Tr} \left[\frac{\partial H}{\partial k_a} \right. \\ &\quad \left. \times G(\omega - \nu, \mathbf{k} - \mathbf{q}/2) \frac{\partial H}{\partial k_b} G(\omega, \mathbf{k} + \mathbf{q}/2) \right],\end{aligned}\quad (\text{S-24})$$

where the sum over ω is Matsubara sum.

$$\sigma_{ab} = \lim_{\omega \rightarrow 0} \left[-\text{Im}[\pi_{ab}(i\nu)/\nu]_{i\nu \rightarrow \omega + i0^+} \right]. \quad (\text{S-25})$$

For convenience, it is better to write both G and H in terms of the Bloch bands projection operators $P_n(\mathbf{k}) = |n, \mathbf{k}\rangle \langle n, \mathbf{k}|$ (which is possible for fermion bilinear theory) with $|n, \mathbf{k}\rangle$ being the eigenvectors of n th band at momentum \mathbf{k} :

$$H(\mathbf{k}) = \sum_n \epsilon_n(\mathbf{k}) P_n(\mathbf{k}), \quad (\text{S-26})$$

$$G(\omega, \mathbf{k}) = \sum_n \frac{P_n(\mathbf{k})}{i\omega - \epsilon_n(\mathbf{k})}. \quad (\text{S-27})$$

After inserting the expression into Eq. (S-24), we find that only the following term contributes

$$\begin{aligned}\pi_{ab}(i\nu) &= \sum_{\omega} \int \frac{d^2k}{(2\pi)^2} \sum_{n_0, \dots, n_3} \text{Tr} \left[\partial_{k_a} P_{n_0} \right. \\ &\quad \left. \times P_{n_1} \partial_{k_b} P_{n_2} P_{n_3} \frac{\epsilon_{n_0} \epsilon_{n_2}}{(i(\omega - \nu) - \epsilon_{n_1})(i\omega - \epsilon_{n_3})} \right] \\ &= \int \frac{d^2k}{(2\pi)^2} \sum_{n_0, \dots, n_3} \text{Tr} \left[\partial_{k_a} P_{n_0} \right. \\ &\quad \left. \times P_{n_1} \partial_{k_b} P_{n_2} P_{n_3} \frac{\epsilon_{n_0} \epsilon_{n_2} (f(\epsilon_{n_3}) - f(\epsilon_{n_1}))}{i\nu + \epsilon_{n_3} - \epsilon_{n_1}} \right].\end{aligned}\quad (\text{S-28})$$

Here $f(\epsilon)$ is the Fermi distribution function and arises from the Matsubara sum. The sum of n_i runs over band indices. After performing the Tr operation, we end up with the following result

$$\begin{aligned}\pi_{ab}(i\nu) &= \int \frac{d^2k}{(2\pi)^2} \sum_{n, n'} \left[-A_{nn'}^a A_{n'n}^b \frac{f(\epsilon_n) - f(\epsilon_{n'})}{i\nu + \epsilon_n - \epsilon_{n'}} \epsilon_n \epsilon_{n'} \right. \\ &\quad + A_{nn'}^a A_{n'n}^{b*} \frac{f(\epsilon_n) - f(\epsilon_{n'})}{i\nu + \epsilon_n - \epsilon_{n'}} \epsilon_{n'}^2 + A_{nn'}^{a*} A_{n'n}^b \frac{f(\epsilon_n) - f(\epsilon_{n'})}{i\nu + \epsilon_n - \epsilon_{n'}} \epsilon_n^2 \\ &\quad \left. - A_{nn'}^{a*} A_{n'n}^{b*} \frac{f(\epsilon_n) - f(\epsilon_{n'})}{i\nu + \epsilon_n - \epsilon_{n'}} \epsilon_n \epsilon_{n'} \right],\end{aligned}\quad (\text{S-29})$$

where $A_{n, n'}^a = -i \langle n | \partial_{k_a} | n' \rangle$, $A_{n, n'}^{a*} = -i \langle \partial_{k_a} n | n' \rangle$ is the matrix element of ∂_{k_a} . Note only the diagonal elements are the Berry connection. Then we perform an analytic continuation $i\nu \rightarrow \omega + i\eta$, and take the imaginary part of $\pi_{ab}(\omega)/\omega$. In the end, we let $\omega \rightarrow 0$. When we take the imaginary part of $\pi_{ab}(\omega)/\omega$, we have two different contributions:

$$\begin{aligned}\pi_{ab}^{(1)} &= \int \frac{d^2k}{(2\pi)^2} \sum_{n, n'} \left(\text{Im}[-A_{nn'}^a A_{n'n}^b] \right. \\ &\quad \left. \times \text{Re} \left[\frac{f(\epsilon_n) - f(\epsilon_{n'})}{\omega + \epsilon_n - \epsilon_{n'} + i\eta} \epsilon_n \epsilon_{n'} \right] + \dots \right),\end{aligned}\quad (\text{S-30})$$

$$\begin{aligned}\pi_{ab}^{(2)} &= \int \frac{d^2k}{(2\pi)^2} \sum_{n, n'} \left(\text{Re}[-A_{nn'}^a A_{n'n}^b] \right. \\ &\quad \left. \times \text{Im} \left[\frac{f(\epsilon_n) - f(\epsilon_{n'})}{\omega + \epsilon_n - \epsilon_{n'} + i\eta} \epsilon_n \epsilon_{n'} \right] + \dots \right),\end{aligned}\quad (\text{S-31})$$

where \dots denotes the rest three terms. Note that $A_{nn'}^a = -A_{n'n}^{a*}$, $(A_{nn'}^a)^* = A_{n'n}^{a*}$, we find

$$\begin{aligned}\pi_{ab}^{(1)} &= \int \frac{d^2k}{(2\pi)^2} \sum_{n, n'} \left(\text{Im}[-A_{nn'}^a A_{n'n}^b] (f(\epsilon_n) - f(\epsilon_{n'})) \right. \\ &\quad \left. \times \text{Re} \left[\frac{(\epsilon_n - \epsilon_{n'})^2}{\omega + \epsilon_n - \epsilon_{n'} + i\eta} + \frac{(\epsilon_n - \epsilon_{n'})^2}{\omega - \epsilon_n + \epsilon_{n'} + i\eta} \right] \right) \\ &= \int \frac{d^2k}{(2\pi)^2} \sum_{n, n'} \left(\text{Im}[-A_{nn'}^a A_{n'n}^b] (f(\epsilon_n) - f(\epsilon_{n'})) \right. \\ &\quad \left. \times \frac{2\omega(\epsilon_n - \epsilon_{n'})^2}{\omega^2 - (\epsilon_n - \epsilon_{n'})^2} \right).\end{aligned}\quad (\text{S-32})$$

Therefore, after taking the limit $\pi_{ab}^{(1)}/\omega|_{\omega \rightarrow 0}$, we obtain

$$\sigma_{ab}^{(1)} = \int \frac{d^2k}{(2\pi)^2} \sum_{n \neq n'} \text{Im}[A_{nn'}^a A_{n'n}^b] (f(\epsilon_n) - f(\epsilon_{n'})), \quad (\text{S-33})$$

which we can use the relation $\langle n | \partial_{k_a} H(k) | n' \rangle = (\epsilon_n - \epsilon_{n'}) A_{nn'}^a + \delta_{n, n'} \partial_{k_a} \epsilon_n$ to transform into the Streda formula. For $\pi_{ab}^{(2)}/\omega|_{\omega \rightarrow 0}$,

$$\text{Im} \left[\frac{f(\epsilon_n) - f(\epsilon_{n'})}{\omega + \epsilon_n - \epsilon_{n'} + i\eta} \right] = \delta_{n, n'} \delta(\omega) \frac{f(\epsilon_n) - f(\epsilon_n + \omega)}{\omega} \Big|_{\omega \rightarrow 0}. \quad (\text{S-34})$$

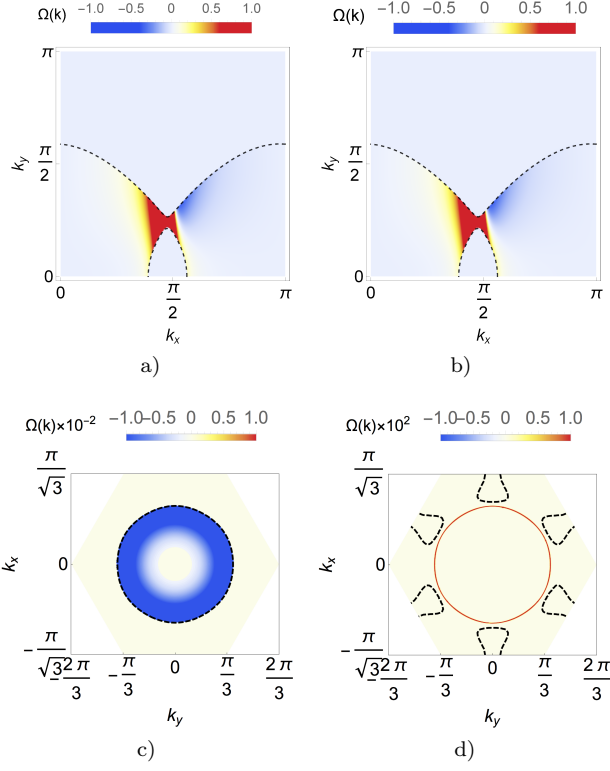


FIG. S2. (Color online) The Berry curvature distributions for the square lattice model, P_S phase (2a) and P_L phase (2b); and for the kagomé lattice model, P_S phase (2c) and P_L phase (2d). The Fermi surfaces are also shown as black dashed lines.

Note that the factor is immediately zero for $n \neq n'$ when we take $\eta \rightarrow 0$. Only $n = n'$ terms survive, and $\pi_{ab}^{(2)}/\omega|_{\omega \rightarrow 0} \sim \delta(\omega)\partial f(\epsilon)/\partial \epsilon$. For $a \neq b$, $\text{Re}[A_{nn}^a A_{nn}^b]$ is symmetric upon exchanging $a \leftrightarrow b$. On the other hand, we know $\pi_{ab} = -\pi_{ba}$. Therefore, $\pi_{ab}^{(2)} = 0$ for $a \neq b$. When $a = b$, we recover the usual Kubo formula result of dc conductivity $\sigma_{xx} \sim \delta(\omega)$.

To show that σ_{xy}^{AH} is a Fermi surface property[4], we can rewrite Eq. (S-33) through an integration by part, and make use of the fact [5] that $\sum_{n'} \text{Im}[A_{nn'}^a A_{n'n}^b] = \nabla_{\mathbf{k}}^a A_{nn}^b - \nabla_{\mathbf{k}}^b A_{nn}^a$:

$$\begin{aligned} \sigma_{ab}^{(1)} &= \int \frac{d^2k}{2\pi^2} \sum_n f(\epsilon_n) (\nabla_{\mathbf{k}}^a A_{nn}^b - \nabla_{\mathbf{k}}^b A_{nn}^a) \\ &= \int \frac{d^2k}{2\pi^2} \sum_n (A_{nn}^b \nabla_{\mathbf{k}}^a f(\epsilon_n) - A_{nn}^a \nabla_{\mathbf{k}}^b f(\epsilon_n)) \quad (\text{S-35}) \\ &= \sum_n \frac{1}{2\pi^2} \oint A_n^a(\mathbf{k}_F) d\mathbf{k}_{Fa}. \end{aligned}$$

Berry curvature distribution

The Berry curvature distributions are shown in Fig. (S2) for the P_S phase (S2a) and P_L phase (S2b)

of the square lattice model, as well as the P_S phase (S2c) and P_L phase (S2d) of the kagomé lattice model. For (S2a) and (S2b), despite the visual resemblance, their difference is still significant as shown in Fig. (3a) of the main text.

Reconstruction of Fermi Surfaces

We note that in the Kondo-destroying P_S phase, only the conduction electrons participate in forming the Fermi surface. By contrast, in the Kondo-screened P_L phase, both the conduction electrons and local f -moments are involved in forming the Fermi surface [7]. In the case of the $J_1 - J_2$ model, the spinon excitations of the CSL phase are gapped. By contrast, in the kagomé case, they are gapless.

To illustrate the point, we show the projected density of states (DOS) in Fig. (S3). The parent spinon TRSB flux state is gapped at zero energy (referred to as “ E_F ”) for the $J_1 - J_2$ case, but is gapless at E_F for the Kagomé case. The DOS structure of the spinons survives the P_L phase (bottom row), but are constrained to straddle E_F . The Fermi surface is only affected in the Kagomé lattice.

This can be seen by directly plotting the Fermi surfaces. Fig. (S4) shows both the Kondo-destroyed and the Kondo-screened phases for both the square lattice model and the kagomé lattice model. It is seen that, for the $J_1 - J_2$ model on the square lattice, the Fermi surface smoothly evolves through the QCP. By contrast, for the kagomé lattice, the Fermi surface experiences a sudden jump across the QCP. We also note that the jump is very substantial. This is because, in the kagomé lattice’s CSL state, the middle spinon band happens to be a flat band.

Analysis of the wavefunction reconstruction across the QCP

To further our understanding about the nonanalyticities across the QCP, we rewrite the Hamiltonian across the QCP in terms of the d -band and f -band eigenstates, which we denote as $|\phi_{\mathbf{k}}^d\rangle$ and $|\phi_{\mathbf{k}}^f\rangle$ respectively:

$$\begin{aligned} H &= \\ &= \sum_{\mathbf{k}} \begin{pmatrix} (\epsilon_{\mathbf{k}}^d - \mu + \lambda') |\phi_{\mathbf{k}}^d\rangle \langle \phi_{\mathbf{k}}^d| & \delta |\phi_{\mathbf{k}}^d\rangle \langle \phi_{\mathbf{k}}^f| \\ \delta |\phi_{\mathbf{k}}^f\rangle \langle \phi_{\mathbf{k}}^d| & (\epsilon_{\mathbf{k}}^f - \mu - \lambda') |\phi_{\mathbf{k}}^f\rangle \langle \phi_{\mathbf{k}}^f| \end{pmatrix}. \end{aligned} \quad (\text{S-36})$$

Here, δ is the hybridization strength. In addition, λ' is the Lagrangian multiplier, which is shifted from λ by a constant that can be absorbed into μ , to obtain the above symmetric form for later convenience. The hybridization, thus the wavefunction reconstruction, is the strongest at the \mathbf{k} points where the conduction bands and spinon bands intersect, i.e., $\epsilon_{\mathbf{k}_0}^f - \mu = \epsilon_{\mathbf{k}_0}^d - \mu = 0$.

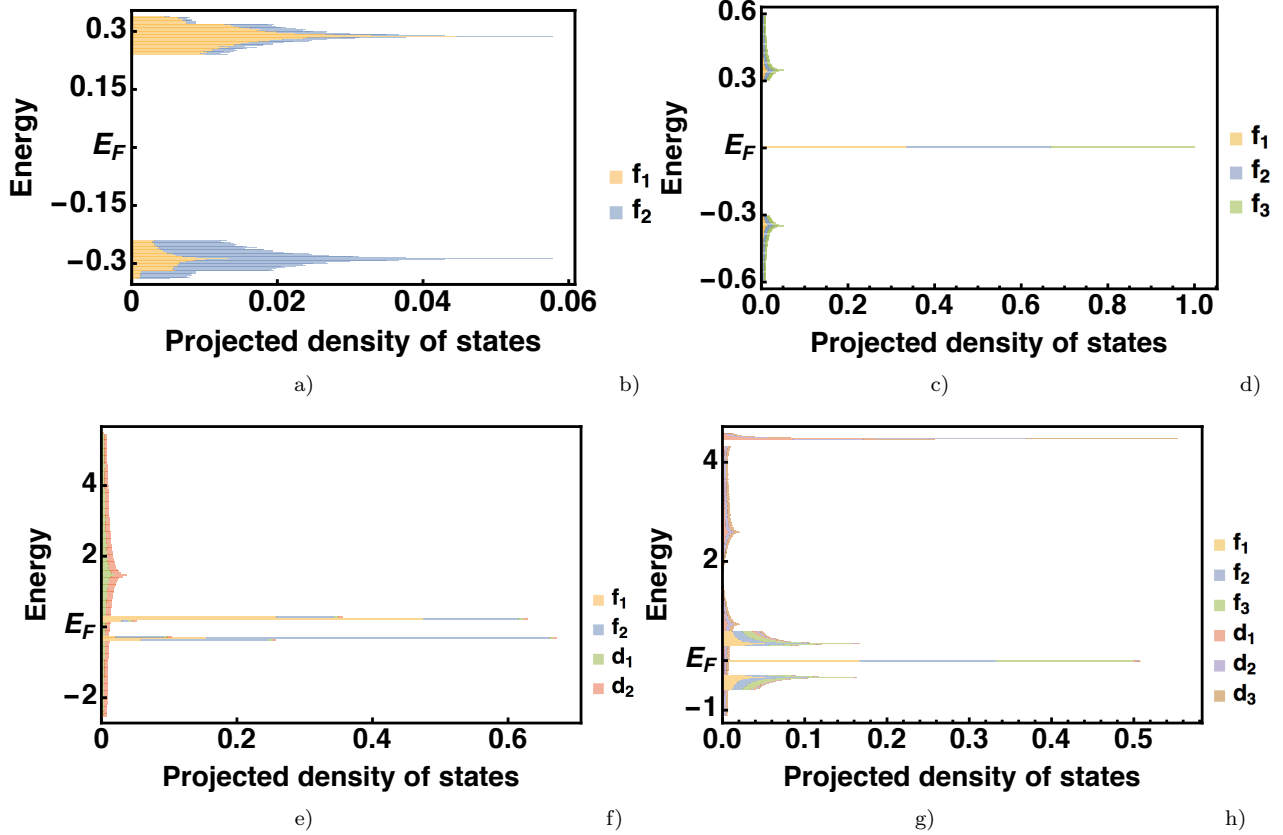


FIG. S3. Density of states projected to the sites of a unit cell, for (a) $J_1 - J_2$ model's spinons in its CSL state, (c) kagomé lattice model's spinons in the $(\frac{\pi}{2}, -\pi)$ state, (e) Kondo screened phase of the $J_1 - J_2$ model, (g) Kondo screened phase of the kagomé lattice model; (b),(d),(f), and (h) shows the relevant legends for color corresponding to the original eigenfunction elements.

For the kagomé case, consider the case that the Fermi surface jumps. We expect λ' to track δ as the QCP is approached. Nonetheless, we can still start out with the points where $\epsilon_{\mathbf{k}_0}^f - \mu = \epsilon_{\mathbf{k}_0}^d - \mu = 0$. In this case, we can write the λ' term as $\lambda' \sigma_0 \otimes \tau_z$, where τ_z is the Pauli matrix for the orbital space. This term does not commute with the hybridization term, which is off-diagonal in the τ space. (Note that both the diagonal and off-diagonal blocks above are diagonal matrices in the sublattice space, and therefore commute with each other in that space.) Therefore, the presence of any λ' prevents us from block-diagonalizing the Hamiltonian even for infinitesimal δ . The new eigenstates are, therefore, reconstructed completely.

Phase diagram in the saddle-point analysis

To illustrate our procedure, we consider the phase diagram arising from the saddle-point analysis in the case of $J_1 - J_2$ square lattice. We minimize the total energy of Eq. (2) with respect to the amplitudes of the link fields ρ_{ij} and $\rho_{K,i}$. The phase diagram of the square lattice model is shown in Fig. (S5), where the red (solid) and

blue (dashed) lines, respectively, mark a first-order phase transition and a crossover. It shows that both the flux-state and the chiral-state solutions can be stabilized, i.e. having lower energies than the unhybridized phase, for J_K larger than some critical $J_{K,c}$. The flux phase solution has the lowest energy when stabilized, signaling that the Kondo coupling favors the gapless states.

For the pyrochlore lattice, the CSL state is gapless [8], and our result here strongly suggests that a similar chiral state could be the ground state on the pyrochlore lattice when the Kondo coupling is introduced.

Potential experimental realization of the frustrated $J_1 - J_2$ Kondo lattice

We suggest the golden phase of SmS (g -SmS) as a promising candidate material. A lattice plane is shown in Fig. (S6). g -SmS shows characteristics of a Kondo insulating state in transport, thermodynamics, and point contact spectroscopy. At temperatures low compared to this scale, the proposed lattice plane could serve as a setting to realize the frustrated $J_1 - J_2$ Kondo lattice and study the anomalous Hall effect.

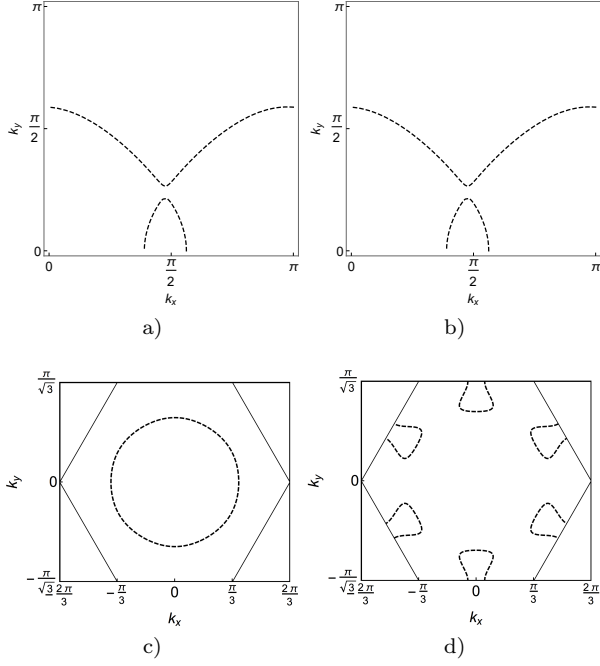


FIG. S4. The Fermi surfaces of the square lattice model in the P_S phase (4a) and in the P_L (4b) phase, and of the Kagomé lattice model in the P_S phase (4c) and in the P_L phase (4d).

- [1] S. Florens and A. Georges, Phys. Rev. B **70**, 035114 (2004).
 [2] S. Florens and A. Georges, Phys. Rev. B **66**, 165111 (2002).

- [3] W. Ding, R. Yu, Q. Si, and E. Abrahams, Phys. Rev. B **100**, 235113 (2019).
 [4] F. D. M. Haldane, Phys. Rev. Lett. **93**, 206602 (2004).
 [5] K. Sun and E. Fradkin, Phys. Rev. B **78**, 245122 (2008).
 [6] S. Paschen, T. Lühmann, S. Wirth, P. Gegenwart, O. Trovarelli, C. Geibel, F. Steglich, P. Coleman, and Q. Si, Nature **432**, 881 (2004).

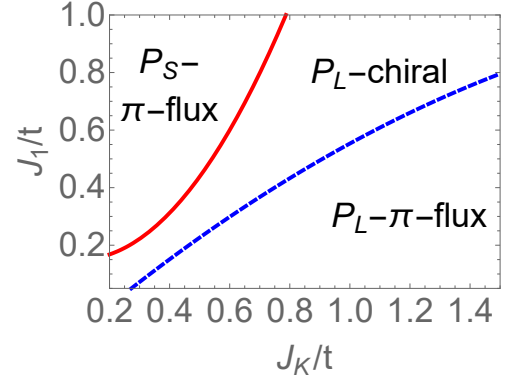


FIG. S5. (Color online) The phase diagram of the $J_1 - J_2 - J_K$ model with $J_2 = J_1/2$ and $n_d = 0.5$ (S5).

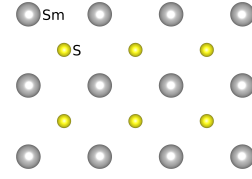


FIG. S6. Lattice plane of g -SmS.

- [7] M. Oshikawa, Phys. Rev. Lett. **84**, 3370 (2000).
 [8] F. J. Burnell, S. Chakravarty, and S. L. Sondhi, Phys. Rev. B **79**, 1 (2008).